Supporting Information

Unraveling electrochemo-mechanical aspects of core–shell composite cathode for sulfide based all-solid-state batteries

Su Cheol Han,‡[a] Mukarram Ali,‡[a,b] Yoon Jun Kim,[a,e] Jun-Ho Park,[a,b] You-Jin Lee,[a] Jun-Woo Park,[a,b]

Heetaek Park,[a] Gumjae Park,[a] Eungje Lee,[c] Byung Gon Kim, [d*] and Yoon-Cheol Ha[a,b*]

[a] Battery Research Division, Korea Electrotechnology Research Institute (KERI), Changwon 51543, Republic of Korea

[b] Department of Electric Energy Materials Engineering, University of Science and Technology (UST), Changwon 51543, Republic of Korea

[c] Chemical Sciences and Engineering Division, Argonne National Laboratory (ANL), Lemont, IL 60439, USA

[d] Department of Applied Chemistry, College of Applied Sciences, Kyung Hee University, Yongin 17104, Republic of Korea

[e] School of Materials Science and Engineering, Pusan National University, Busan 46241, Republic of Korea

* Corresponding authors

Byung Gon Kim (byunggonkim@khu.ac.kr) and Yoon-Cheol Ha (ycha@keri.re.kr)

‡ These authors contributed equally

Experimental Details

Preparation of Li₆PS₅Cl and LNO@NMC

An argyrodite solid electrolyte, Li_6PS_5Cl (LPSCl), with a particle size of 3 μm, was sourced from CISOLID, Korea. The ionic conductivity of LPSCl was 1.45 mS/cm, as shown in **Figures S9A** and **S9B**. The X-ray diffraction (XRD) data indicated that the LPSCl SSE had high crystallinity with minimal Li_2S impurity phase (see **Figure S9C**). The particle size of the CISOLID LPSCl ranged from 1 to 3 μm (**Figure S9D**).

The commercial $LiNi_{0.8}Mn_{0.1}Co_{0.1}O_2$ (NMC) powder used in this study was procured from Ecopro BM, Korea. The $LiNbO_3$ (LNO) coating layer was developed from an alcoholic solution of Li and Nb alkoxides in accordance with a procedure reported in a previous study.[1] 0.325 g (0.046 mol) of metallic Li and 14.58 g (0.046 mol) of $Nb(C_2H_5O)_5$ were dissolved in 188 mL of anhydrous ethanol (C_2H_6O) at 25 °C under an Ar gas atmosphere. The molar ratio of Li and niobium ethoxide was maintained at 1:1. The prepared solution was sprayed on 1 kg of NCM powder at a rate of 2 g/min using a rolling fluidized bed coater (MP-01, Powrex). The LNO-coated sample was heated at 400 °C for 30 min under an O_2 flow post-coating.

Blade grinding and blade milling of LPSCl@LNO@NMC

The LNO@NMC powders and LPSCl were processed using a specially designed Ar-filled blade mill (BM) system (KMTech, Blade Mill, 001; **Figure S1**) to minimize the adverse effects of moisture and O. In this setup, the LNO@NMC and LPSCl served as the host and guest particles of the composite, respectively. A detachable vessel was equipped to transfer the powders between the BM system and an Ar-filled glove box. During the BM process, both the host and guest particles were propelled against the inner wall of the vessel at 4000 RPM. Owing to the centrifugal force generated by the rotating blade, the particles were propelled through the narrow space between the stationary press-head and the inner wall of the vessel and were subjected shear and compression forces. This process was repeated

15 times, with each cycle comprising 60 s of operation and 90 s rest. The system temperature was maintained at 15 °C throughout to prevent overheating of the BM chamber and mitigate any side reactions. Consequently, a uniformly coated, thin solid electrolyte layer was formed with a core–shell SSE@LNO@NMC. This process facilitated the uniform coating of smaller guest particles (SSEs) onto larger host particles (LNO@NMC), eliminating the need for binders or solvents.

For the 5 wt.% LPSCl-coated LPSCl@LNO@NMC (BM-05), the LNO@NMC and LPSCl powders were loaded into the BM vessel at a weight ratio of 95:5, yielding a total weight of 40 g (approximately 50 mL in volume). The vessel was then sealed in an Ar-filled glove box. The BM process was conducted at a controlled temperature of 15 °C, managed by a programmed cooling system attached to the head of the BM chamber. Because the BM−05 LPSCl@LNO@NMC composite was fabricated via a BM process in an Ar-sealed environment within a short period, it did not significantly impact the properties of the LPSCl coating on the NMC surface. The 3 wt.% (BM−03) and 10 wt.% BM−10 samples were fabricated similarly.

Material Characterization

Morphological analysis of the multi-core–shell LPSCl@LNO@NMC powders was conducted using a field-emission scanning electron microscope (FE-SEM, Hitachi S4800). The structure and crystalline phase of the powders were investigated via XRD using a Philips/PANalytical X-pert PRO MPD instrument with Cu Kα radiation (wavelength, $\lambda = 0.15406$ nm) at a scan rate of 8 min^{-1} and a step size of 0.026°.

The electronic states of the elements were characterized via X-ray photoelectron spectroscopy (XPS, Kα + XPS System, Thermo Scientific, Loughborough, UK). XPS was conducted with a monochromatic Al Kα source (hυ = 1486.6 eV) and a spot size of 400 μm. Cross-sectional analysis of both the LNO@NMC and LPSCl@LNO@NMC samples was performed using focused ion beam-energy dispersive X-ray spectroscopy (FIB-EDS) analysis. An FIB-crater was milled using a Thermo-fisher Helios 5CU, and EDS was conducted using an Oxford ULtim-100 in a cryo-chamber. Transmission electron microscopy (TEM) was conducted using a TECNAI G2 F20 (80~200 kV)

coupled with high-angle annular dark-field (HAADF) scanning EDS. Because the microstructure is readily changed because of the electron beam energy of the TEM instrument, the measurement power was decreased to 80 kV. The void and porosity of both LNO@NMC and the 5–BM LPSCl@LNO@NMC-based composite cathodes were analyzed via cross-sectional polished (CP) scanning electron microscopy-energy dispersive X-ray spectroscopy (SEM-EDS) using a Gatan Ilion-II 297. The composite pellets were milled at a rate of 300 μm/h at a potential of 8.0 kV. The ion current density was set to 10 mA/cm². The entire process was conducted in an Ar environment.

Electrochemical Characterization

The ionic conductivities of the CISOLID SSE powders were evaluated via electrochemical impedance spectroscopy (EIS). A symmetric cell with an In |SSE| In (In = Indium foil) configuration was assembled using a commercial press cell jig (TLP11909-S, Teraleader, Korea). Next, 200 mg of the SSE powder was compressed using martensitic steel plungers at 350 MPa for 60 s in a 10-mm-diameter alumina mold. After removing the plungers, a 50-μm-thick In foil was affixed to both sides of the pellet, serving as an ion-blocking electrode. The mold was sealed with stainless steel rods, which acted as current collectors, and pressed again at 20 MPa for 5 s. Finally, the assembly was mounted in the press cell jig and a torque of 5 N·m was applied using a torque wrench. EIS analysis was conducted in the frequency range from 1 MHz to 100 mHz. The activation energy (E_a) of the SSE pellet was evaluated via EIS over the temperature range of 25–60 °C.

Li | SSE | composite | SSE | Li was fabricated to measure the ionic conductivity of the composite cathode. First, 100 mg of the cathode composite was transferred into an alumina cell with an inner diameter of 10 mm and compressed using martensitic steel plungers at 200 MPa for 60 s. Next, 60 mg of SSE powder was added to each side of the cathode composite and pressed at 200 MPa for 60 s. After removing the plungers, a 20-μm-thick Li foil was affixed to both sides of the pellet, serving as a Li source. The theoretical density of the composite cathode was calculated by assuming that the bulk densities of LPSCl, NCM811, and vertically grown carbon fibers (VGCFs) were 1.64, 4.8, and 2 g cm^{-3}, respectively. The volume fraction of NMC811 active material was adjusted to 51.1% for all the

4

samples. EIS analysis was conducted in the frequency range from 7 MHz to 100 mHz before and after cycling.

To analyze the charge–discharge performance and internal pressure, all-solid-state Li cells were fabricated using a commercial press cell jig (TLP11909-S and TLP1109-L, Teraleader, Korea). Initially, a composite cathode powder was prepared by blending bare and BM powders, CISOLID SSE, and VGCFs. For all the tests, the NMC811 active material:SSE:VGCF ratio was maintained at 75:22:3. This mixture was then agitated in a Thinky mixer (Thinky, USA) with 5 mm ZrO_2 balls at 1800 RPM for 3 min to yield the final cathode composite. Subsequently, a Li–In alloy anode was prepared by pressing In and Li foils together.

The composite cathode |SSE| Li–In cell was assembled as follows: 120 mg of the CISOLID SSE powder was loaded into a 10 mm alumina mold and compacted with martensite rods at 350 MPa for 60 s. After removing the rods, 10 mg of the composite cathode powder was spread uniformly on one side of the SSE pellet and pressed again at 350 MPa for 60 s. The Li–In foil was then attached to the other side, and the mold was sealed using martensite rods as current collectors. The entire structure was compressed at 20 MPa for 5 s. The assembly was carefully mounted in the press cell jig, and a torque of 5 N·m (12.7 MPa) was applied using a torque wrench. The active material loading level was maintained within 9–10 mg/cm².

Electrochemical galvanostatic cycling of the all-solid-state lithium-ion batteries (ASSLBs) was conducted at a C-rate of 2 C for 1000 cycles, with an initial cycle at 0.1 C to calculate the initial discharge capacity. This process was performed at a constant temperature of 55 °C. Galvanostatic rate cycling was executed at 0.1, 0.2, 0.3, 0.5, 1, and 2 C (assuming 1 C = 200 mA/g), with each rate applied for five cycles at a constant temperature of 55 °C. For all cells, the voltage window for cycling was set to 2.0–3.7 V versus In (2.6–4.3 V versus Li). To examine the stack pressure evolution at open circuit and electrochemical cycling, a similar cell fabrication process was followed, and a special cell assembly (TLP1109-L, Teraleader, Korea; **Figure S7A**) was employed wherein a pressure change sensor was connected at the bottom of the cell. During the stack pressure analysis, the stack pressure data was calibrated using software, and the stack pressure evolution was analyzed for 90 cycles (2 C).

Charging and discharging occurred in constant current mode. EIS analysis before and after cycling was conducted in the frequency range from 200 kHz to 100 mHz.
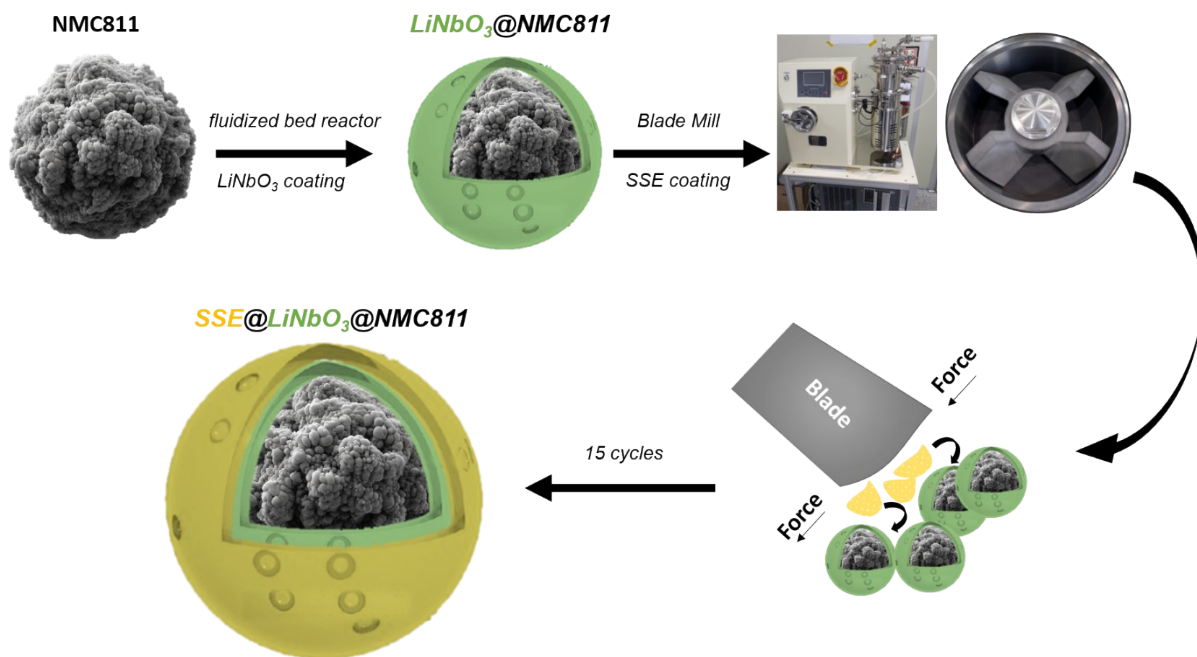
Figure S1. Schematic of the core-shell CAM particles fabrication process.
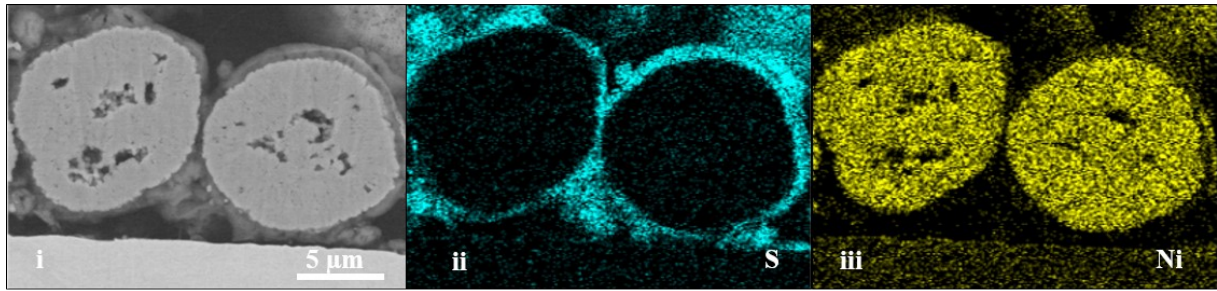
Figure S2. CP-SEM image and EDS maps of BM−05 SSE@LNO@NCM811 powders.

As shown in **Figure S2**, the BM−05-based composite exhibits a dense microstructure, and the interface of the active material is well percolated with SSE.

The theoretical shell thickness is calculated follows:

$$\frac{\frac{4}{3}\pi (r + x)^3 - \frac{4}{3}\pi r^3}{\frac{4}{3}\pi r^3} = \frac{M_{LPSCl}}{M_{LNO@NCM}} \times \frac{\rho_{NCM}}{\rho_{LPSCl}},$$

where r is the mean radius of the LNO@NMC particle, x is the shell thickness, and ρ is the theoretical density (ρ_{NCM} = 4.8 g/cm^3, p_{LPSCl} = 1.64 g/cm^3); M_{LPSCl} denotes the weight of LPSCl and M_{NMC} is the weight of NMC used in the BM process. The calculated theoretical shell thickness was approximately 516 nm for 5 wt.% LPSCl@LNO@NMC. The average measured thickness of the LPSCl shell obtained via CP analysis was 474 nm.
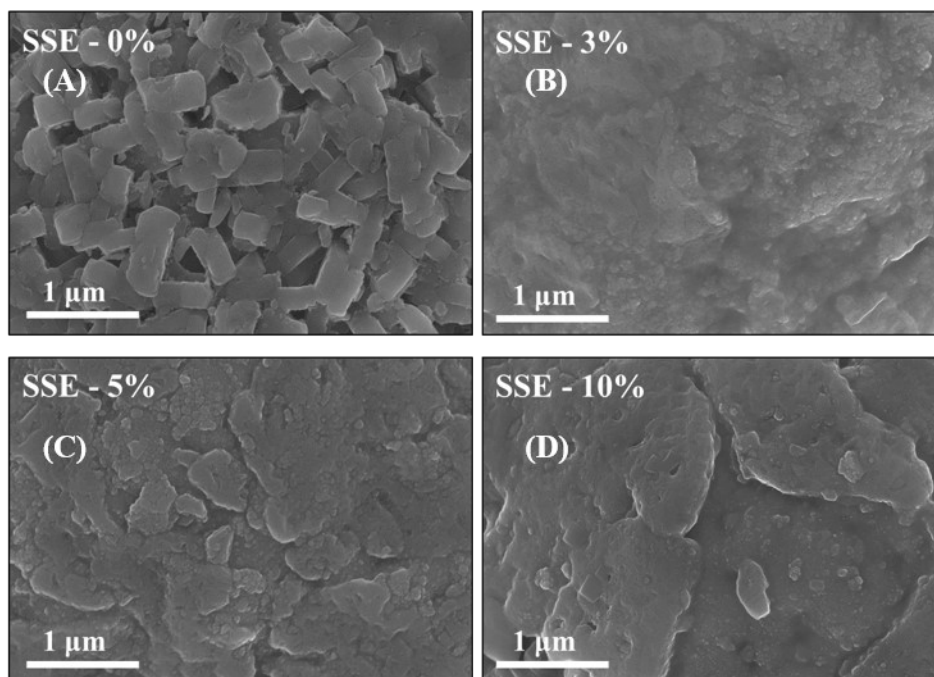
Figure S3. FE-SEM images of the LNO@NMC **(A)**, BM-03 **(B)**, BM-05 **(C)**, and BM-10 **(D)** samples.
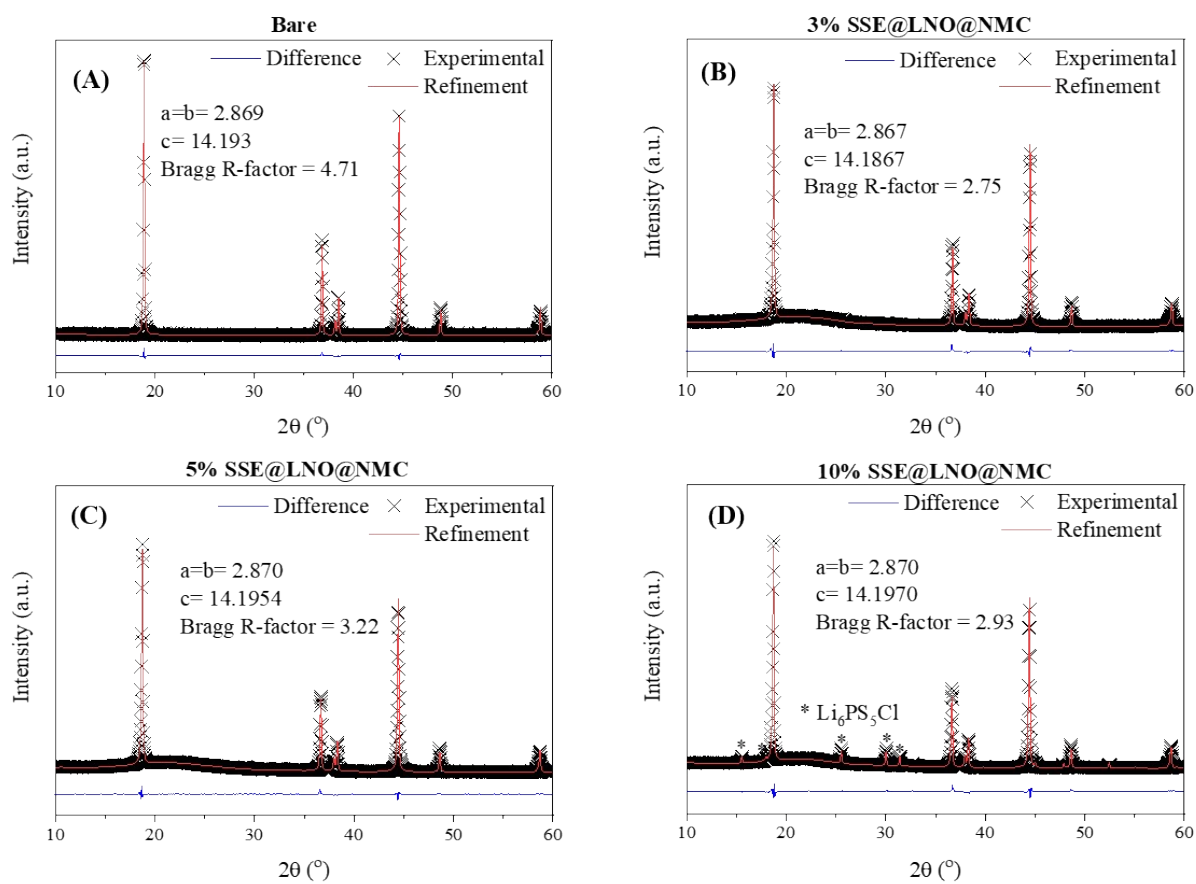
Figure S4. XRD and Rietveld refinement plots for the LNO@NMC **(A)**, BM−03 **(B)**, BM−05 **(C)**, and BM−10 **(D)** samples.
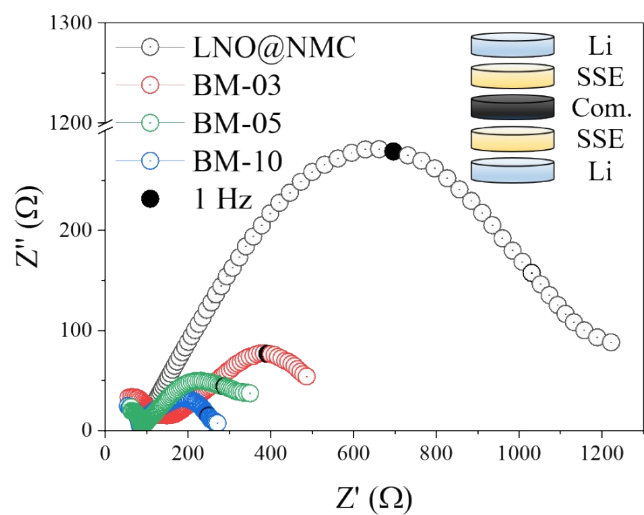
Figure S5. Results of the EIS analysis of Li | SSE | Composite | SSE | Li cells of the LNO@NMC, BM-03, BM-05, and BM-10 composite cathodes. The ionic conductivity and tortuosity factors of the composite cathodes were calculated in accordance with the method described in a previous report.[2]

(A)

(B)

(C)
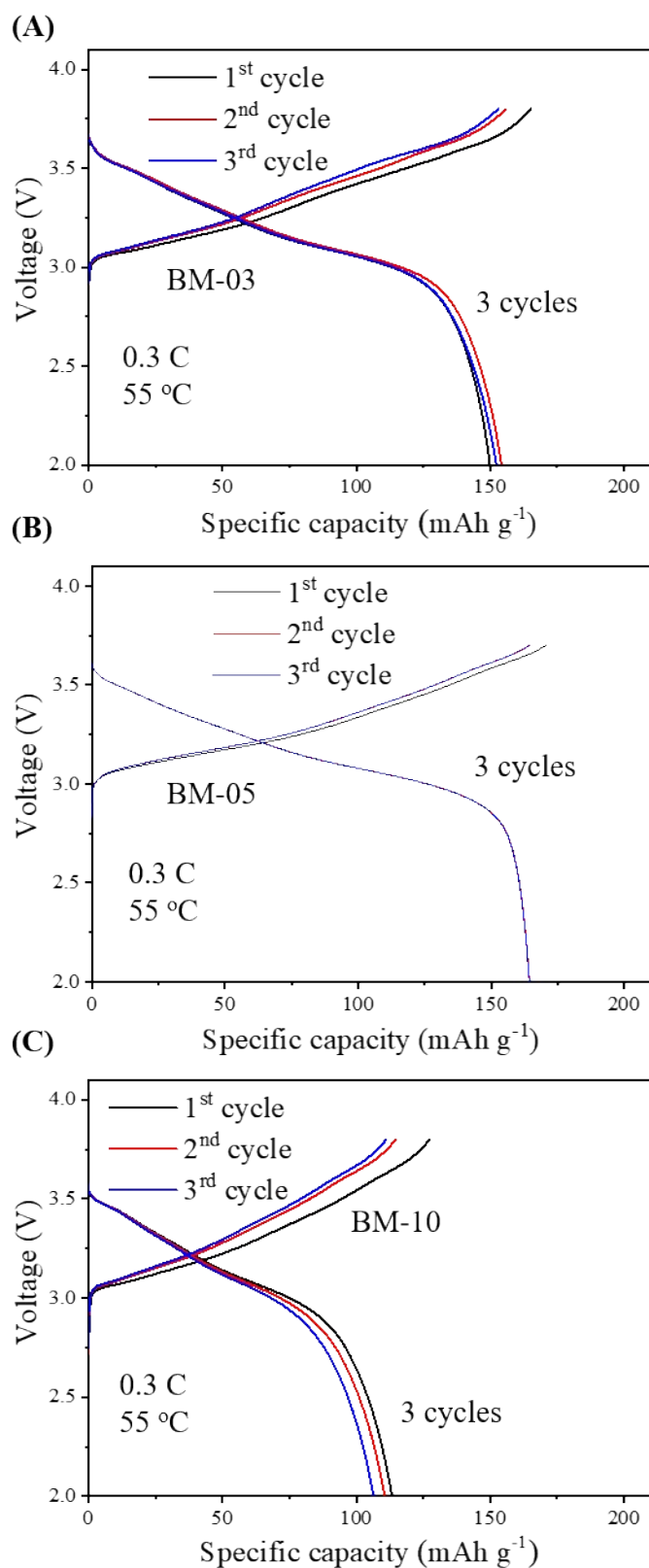
Figure S6. Galvanostatic charge–discharge profiles of the BM-03- **(A)**, BM-05- **(B)**, and BM-10- **(C)** based composite cathodes in ASSLBs.
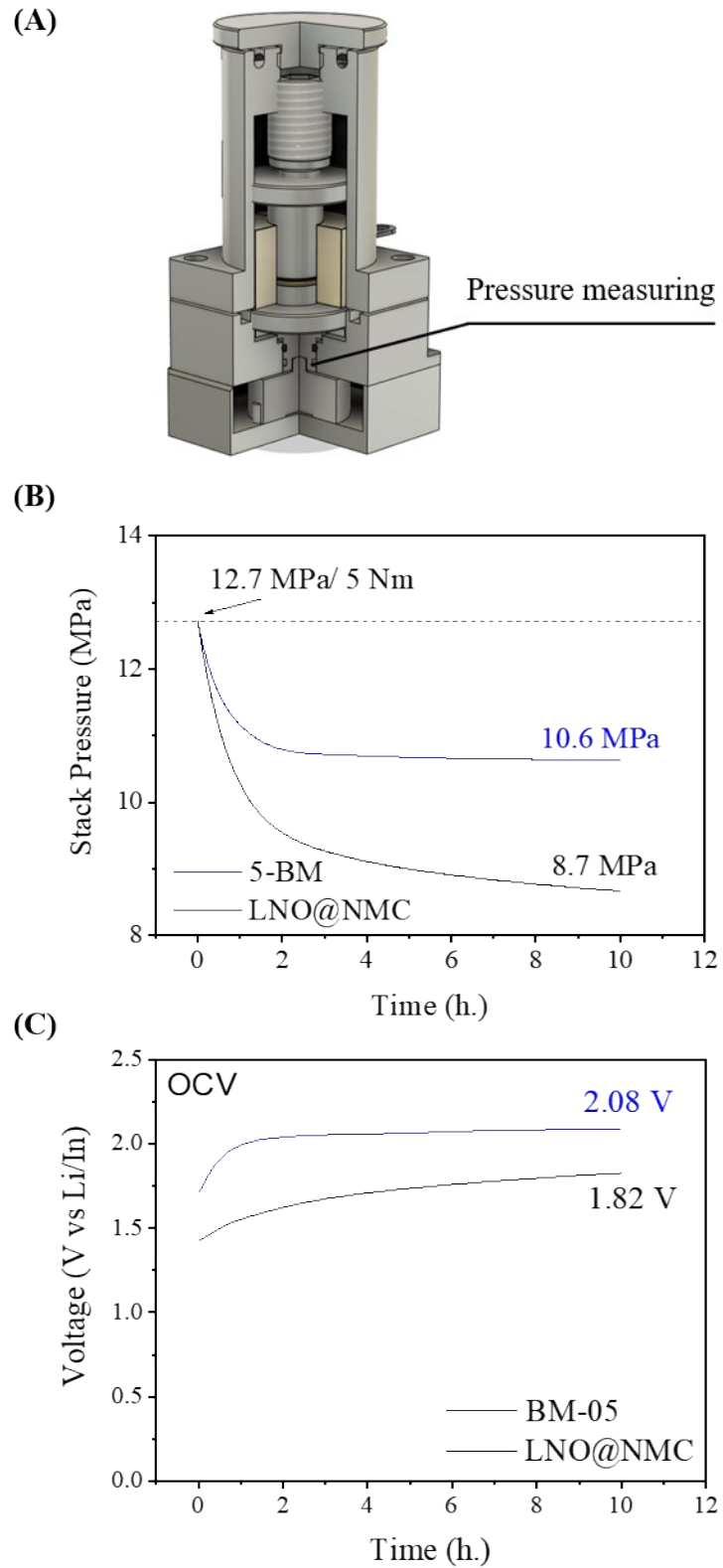
Figure S7. (A) Pressure analysis cell configuration used in this study. **(B)** Stack pressure evolution of the BM−05 SSE@LNO@NMC | SSE | Li/In and bare LNO@NMC | SSE | Li/In cells at open circuit for 10 h. **(C)** Open circuit voltage change during rest time for 10 h.
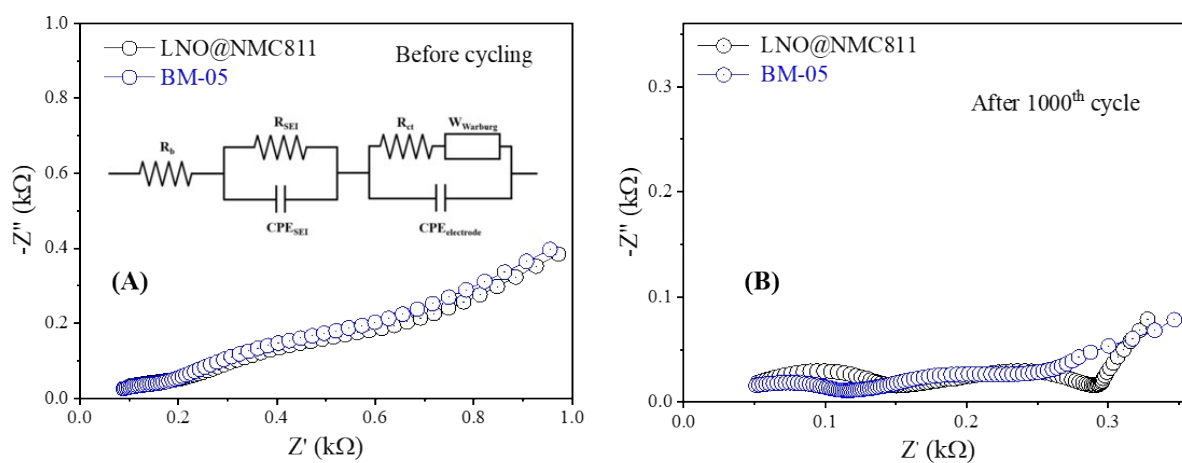
Figure S8. EIS analysis results obtained before and after cycling for LNO@NMC-based **(A)** and BM-05-based **(B)** ASSLBs.
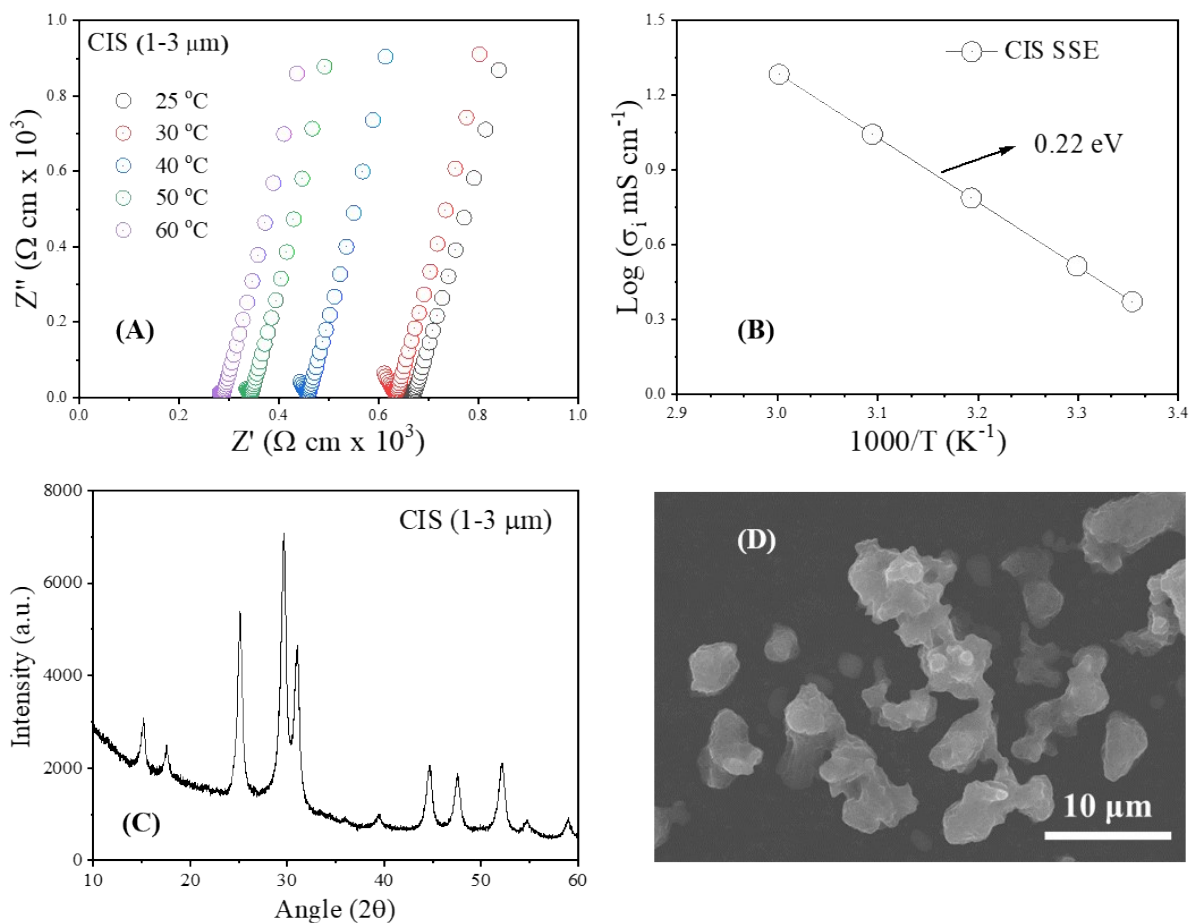
Figure S9. (A) Results of temperature-dependent EIS for evaluating the ionic conductivity of CISOLID LPSCl powder. **(B)** Arrhenius plot of CISOLID LPSCl for evaluating E_a. **(C)** FE-SEM image of LPSCl powder. **(D)** XRD analysis results of the LPSCl powder.

The ionic conductivity of LPSCl was evaluated to be 1.45 mS/cm, and E_a was calculated to be 0.22 eV. The SEM analysis results show that the particle size ranged from 1 μm to 3 μm.

Table S1. Summary of the BM process and electrochemical analysis results.

Parameter	Unit	Value
Details of mechano-fusion		
NCM:LPSCl (Bare) (BM)	wt.%	100:00
NCM:LPSCl (BM-03) (BM)	wt.%	95:03
NCM:LPSCl (BM-05) (BM)	wt.%	95:05
NCM:LPSCl (BM-10) (BM)	wt.%	95:10
BM time	s	60
BM rest time	s	90
No. of cycles	n	15
Details of composite cathode		
CAM: SSE: VGCF	wt.%	75:22:3
Loading level	mg cm^{-2}	9–10
Cathode thickness (LNO@NMC811) *	μm	~51.6
Cathode density (LNO@NMC811) *	g cm^{-3}	2.43
Cathode thickness (BM-05)	μm	~46.7
Cathode density (BM-05)	g cm^{-3}	2.72
Ionic conductivity of composite cathode		
Ionic conductivity (LNO@NMC – composite)	mS cm^{-1}	5.3×10^{-5}
Ionic conductivity (BM-03 – composite)	mS cm^{-1}	1.3×10^{-4}
Ionic conductivity (BM-05 – composite)	mS cm^{-1}	1.8×10^{-4}
Ionic conductivity (BM-10 – composite)	mS cm^{-1}	1.9×10^{-4}
Ionic tortuosity factors (LNO@NMC – composite)	τ^2_{ion}	6.7
Ionic tortuosity factors (BM-03 – composite)	τ^2_{ion}	2.0
Ionic tortuosity factors (BM-05 – composite)	τ^2_{ion}	1.8
Ionic tortuosity factors (BM-10 – composite)	τ^2_{ion}	1.6
EIS details before and after cycling		
Interfacial resistance (R_i) before cycling (LNO@NMC)	Ω	31.1
Interfacial resistance (R_i) before cycling (BM-05)	Ω	36.7
Interfacial resistance (R_i) after cycling (LNO@NMC)	Ω	148
Interfacial resistance (R_i) after cycling (BM-05)	Ω	109
Charge transfer resistance (R_{ct}) after cycling (LNO@NMC)	Ω	291
Charge transfer resistance (R_{ct}) after cycling (BM-05)	Ω	236

* The composite cathode thickness was obtained by averaging the measurements of 10 samples

Table S2. Reported specific capacities at various current densities for wet- and dry-coated multi-core–shell cathode active materials for ASSLBs.

*Cathode material	Coating type	Coating material	Loading level $mg\ cm^{-2}$	Current rate C	Specific capacity $mAg\ g^{-1}$	Ref
NMC811	dry	Li_6PS_5Cl	1.5	0.05	165	3
				0.1	158	
				0.2	100	
				0.5	50	
LZO@NMC811	dry	$Li_{10}SnP_2S_{12}$	20	0.1	192	4
				0.5	155	
NMC9XX	wet	Li_3BO_4	11	0.1	207	5
				0.6	180	
				1	155	
				2	130	
				4	74	
NMC622	wet	$Li_{1.4}Al_{0.4}Ti_{1.6}(PO_4)_3$	7	0.05	158	6
				0.1	150	
				0.2	138	
				0.5	120	
				1	95	
NMC333	wet	Li_6PS_5Br	18	0.5	119	7
LCO	wet	$LiNbO_3$	10	0.1	80	1
				0.5	68	
				1	55	
				2	39	
				5	8	
LNO@NMC333	dry	Li_3PS_4	10	0.05	150	8
				0.2	138	
LNO@NMC333	dry	Li_3PS_4	10	0.5	100	8
				1	85	
				2	40	
				5	10	
NMC811	wet	Li_3InCl_6	10	0.05	138	9
				0.1	121	
				0.2	95	
				0.2	80	
NMC811	wet	Li_3InCl_6	13	0.1	158	10
				0.2	130	
				0.3	120	
				0.5	110	
				1	95	
LNO@LCO	PLD	Li_3PS_4	10	0.1	95	11
LNO@LCO	wet	Li_6PS_5Cl	18	0.1	50	12
LCO	wet	Li_6PS_5Cl	12	0.05	60	13
				0.1	50	
				0.2	38	
				0.5	25	
				1	18	
LNO@LCO	wet	Li_3PS_4	9	0.1	110	14

LNO@LCO	PLD	$3Li_4GeS_4 \cdot 67Li_3PS_4$	15	0.1	85	15
LNO@LCO	wet	Li_4SnS_4	12	0.1	138	16
				0.2	135	
				0.5	120	
				0.7	110	
				1	95	
				2	60	
LNO@LCO	wet	Li_4SnS_4	12	5	10	16
LCO	wet	Li_3PS_4	18	0.05	113	17
LNO@NMC811	**dry**	**Li_6PS_5Cl**	**10**	**0.1**	**197**	***This work***
				0.3	**176**	
				0.5	**167**	
				1	**144**	
				2	**112**	

* $LiCoO_2$ (LCO), $LiNbO_3$ (LNO), $LiNi_{0.8}Mn_{0.1}Co_{0.1}O_2$ (NMC811), $LiNi_{0.6}Mn_{0.2}Co_{0.2}O_2$ (NMC622), $LiNi_{0.9X}Mn_{0.0X}Co_{0.0X}O_2$ (NMC9XX), $LiNi_{1/3}Mn_{1/3}Co_{1/3}O_2$ (NMC333), pulsed laser deposition (PLD)

References

1   N. Ohta, K. Takada, I. Sakaguchi, L. Zhang, R. Ma, K. Fukuda, M. Osada and T. Sasaki, *Electrochem. Commun.*, 2007, **9**, 1486.

2   P. Minnmann, L. Quillman, S. Burkhardt, F. H. Richter and J. Janek, *J. Electrochem. Soc.*, 2021, **168**, 040537.

3   J. Kim, M. J. Kim, J. Kim, J. W. Lee, J. Park, S. E. Wang, S. Lee, Y. C. Kang, U. Paik, D. S. Jung and T. Song, *Adv. Funct. Mater.*, 2023, **33**, 2211355.

4   Y. Park, J. H. Chang, G. Oh, A. Kim, H. Chang, M. Uenal, S. Nam and O. Kwon, *Small*, 2024, **20**, 2305758.

5   U.-H. Kim, T.-Y. Yu, J. W. Lee, H. U. Lee, I. Belharouak, C. S. Yoon and Y.-K. Sun, *ACS Energy Lett.*, 2023, **8**, 809.

6   X. Li, Z. Jiang, D. Cai, X. Wang, X. Xia, C. Gu and J. Tu, *Small*, 2021, **17**, 2103830.

7   S. Yubuchi, M. Uematsu, C. Hotehama, A. Sakuda, A. Hayashi and M. Tatsumisago, *J. Mater. Chem. A*, 2019, **7**, 558.

8   H. Nakamura, T. Kawaguchi, T. Masuyama, A. Sakuda, T. Saito, K. Kuratani, S. Ohsaki and S. Watano, *J. Power Sources*, 2020, **448**, 227579.

9   Q. Ye, X. Li, W. Zhang, Y. Xia, X. He, H. Huang, Y. Gan, X. Xia and J. Zhang, *ACS Appl. Mater. Interfaces*, 2023, **15**, 18878.

10 J. Wang, S. Zhao, A. Zhang, H. Zhuo, G. Zhang, F. Han, Y. Zhang, L. Tang, R. Yang, L. Wang and S. Lu, *ACS Appl. Energy Mater.*, 2023, **6**, 3671.

11 A. Sakuda, A. Hayashi, T. Ohtomo, S. Hama and M. Tatsumisago, *J. Power Sources*, 2011, **196**, 6735.

12 S. Yubuchi, S. Teragawa, K. Aso, K. Tadanaga, A. Hayashi and M. Tatsumisago, *J. Power Sources*, 2015, **293**, 941.

13 Z. Zhang, L. Zhang, Y. Liu, X. Yan, B. Xu and L. Wang, *J. Alloys Compd.*, 2020, **812**, 152103.

14 S. Teragawa, K. Aso, K. Tadanaga, A. Hayashi and M. Tatsumisago, *J. Power Sources*, 2014, **248**, 939.

15 Y. Ito, M. Otoyama, A. Hayashi, T. Ohtomo and M. Tatsumisago, *J. Power Sources*, 2017, **360**, 328.

16 Y. E. Choi, K. H. Park, D. H. Kim, D. Y. Oh, H. R. Kwak, Y. Lee and Y. S. Jung, *ChemSusChem*, 2017, **10**, 2605.

17 J. Kim, M. Eom, S. Noh and D. Shin, *J. Power Sources*, 2013, **244**, 476.